Pergamon

Int. J. Heat Mass Transfer. Vol. 41, No. 13, pp. 2025–2035, 1998

Printed in Great Britain
0017-9310/98 $19.00+0.00

PII: S0017-9310(97)00256-1

Maximum power from a hot stream

A. BEJAN† and M. R. ERRERA

Department of Mechanical Engineering and Materials Science, Box 90300, Duke University, Durham, NC 27708-0300, U.S.A.

(*Received* 9 *October* 1996 *and in final form* 13 *August* 1997)

Abstract—This paper reports the solution to the fundamental problem of how to maximize the mechanical power extracted from a hot single-phase stream when the total heat transfer area bathed by the stream is constrained. It is shown that the optimization has two degrees of freedom: the shape of the stream temperature distribution as a function of the length (x) traveled along the heat transfer surface, and the position of this distribution on the absolute temperature scale. The optimal stream temperature distribution is exponential in x, and so is the temperature distribution along the hot end of the system that converts the heat transfer into mechanical power. At any x, the temperature difference across the heat exchanger is proportional to the local absolute temperature. Similar conclusions are reached for the cold end heat exchanger, when the power system rejects heat to a cold single-phase stream. It is shown that the optimal solution can be implemented in practice by using two counterflow heat exchangers. Each counterflow is imbalanced to a degree recommended by thermodynamic optimization. The effect of the sizes and capacity rates of the two heat exchangers is documented.

1. BACKGROUND

How to convert heat into work is the question that led to heat engines and the industrial revolution. In this paper we propose that we take a fresh look at this age old question, not from the thermodynamics direction, but from the direction of heat transfer. The combined application of heat transfer and thermodynamics in the optimization of thermal systems has become a self standing and very active field, which is reviewed annually (e.g. refs. [1–5]). Why a fresh look is timely will become clear after re-examining the solved problems shown in Figs. 1–3.

The key observation is that in the thermodynamics of power cycles it is routinely assumed that the energy input is already available as heat transfer. In almost every application, however, the energy input is initially carried into the power plant by a stream—e.g., a mixture of fuel and oxidant, hot products of combustion, exhaust gases, or hot geothermal steam. To convert the stream energy into a heat input for the cycle executed by the working fluid of the power plant is the function of one or more heat exchangers. This overlooked interface between the power cycle (pure thermodynamics) and the stream requires a heat transfer perspective.

Thermodynamics alone provides an unambiguous answer to the question of the maximum power that is theoretically available from a stream solely in the presence of the atmospheric temperature reservoir (T_0): that answer is the 'flow exergy' of the stream (e.g. ref. [7], p. 133). It is helpful to review this result

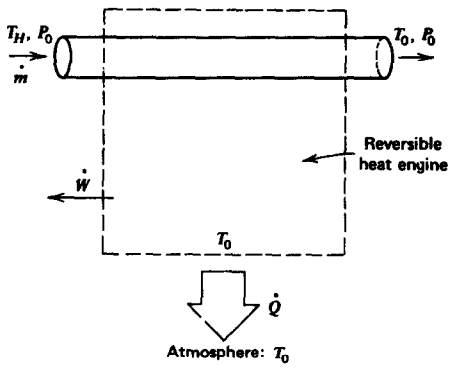

Fig. 1. Power plant model with hot stream cooled reversibly while in contact with the atmospheric temperature reservoir (ref. [6], p. 18).

while looking at Fig. 1 and assuming that the stream is single-phase, for example, an ideal gas or an incompressible liquid. The hot stream ($\dot{m}, T_H$) powers a reversible device, and reaches thermal equilibrium with the ambient before it is discharged. The pressure drop along the stream is assumed negligible. The theoretical power output is (e.g. ref. [6], p. 18):

$$\dot{W}_{\substack{\text{rev}\\ \text{Fig.1}}} = \dot{m} c_p T_0 \left(\frac{T_H}{T_0} - 1 - \ln \frac{T_H}{T_0} \right). \tag{1}$$

The actual power output will always be lower than $\dot{W}_{rev}$ because of the irreversibility of the heat transfer between the hot stream and the rest of the power plant. A first step in the direction of accounting for the heat transfer irreversibility was taken in the model of Fig. 2, where the heat transfer surface has the finite

† Author to whom correspondence should be addressed.

NOMENCLATURE

A	heat transfer area
c_p	specific heat at constant pressure
C_H, C_L	capacity flow rates
L	flow length
$\dot{m}$	mass flow rate
N, N_H, N_L, N_{tu}	numbers of heat transfer units
p	wetted perimeter, or heat transfer surface per unit length
$\dot{Q}_e$	external heat transfer rate
$\dot{Q}_H$	input heat transfer rate
$\dot{Q}_0$	rejected heat transfer rate
$\dot{S}_{gen}$	entropy generation rate
$T(x)$	hot stream temperature distribution, Fig. 4
T_c	cold stream temperature distribution, Fig. 10
T_{cr}	temperature of the cold end of the reversible compartment, Fig. 10
T_h	hot stream temperature distribution, Fig. 10
T_{hr}	temperature of the hot end of the reversible compartment, Fig. 10
T_H	the highest temperature
T_L	the lowest temperature
T_{out}	outlet temperature
T_0	ambient temperature
U	overall heat transfer coefficient based on A
$\dot{W}$	power output
$\hat{W}$	dimensionless power output, equation (32)
$\tilde{W}_{mm}$	dimensionless power output, equation (19)
x	flow coordinate
$\hat{x}$	heat exchanger allocation ratio.

Greek symbols

ε	heat exchanger effectiveness
λ	Lagrange multiplier
μ, μ_H, μ_L	functions
Φ	integral, equation (11).

Subscripts

H	high temperature
L	low temperature
max	maximum
mm	maximized twice
opt	optimal
out	outlet
rev	reversible
s	surface, or working fluid at the hot end, Fig. 4.

thermal conductance UA and uniform temperature T_s. The hot stream enters the heat exchanger at T_H, and mixes with the rest of the fluid to a uniform temperature (T_{out}) while it is cooled by the T_s surface. The spent stream is discharged at the same temperature, T_{out}. The rest of the power plant is modeled as reversible.

It was shown in ref. [7], pp. 381–385, that in Fig. 2

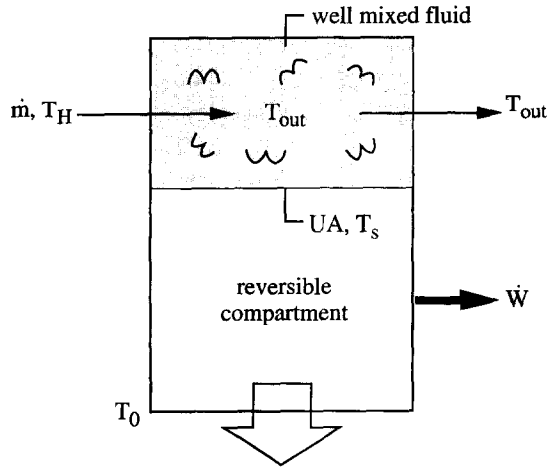

Fig. 2. Power plant model with hot stream, well mixed fluid in contact with isothermal heat transfer surface (T_s), and reversible compartment (ref. [7], p. 382).

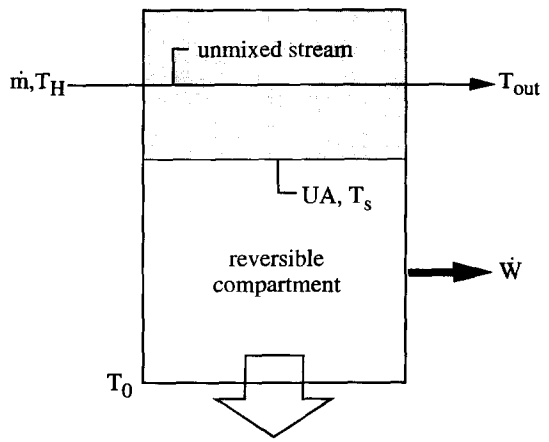

Fig. 3. Power plant driven by an unmixed hot stream in contact with an isothermal heat transfer surface (ref. [8], p. 197).

the power output $\dot{W}$ has a maximum with respect to the temperature of the heat transfer surface. This degree of freedom (T_s) is available in the design of the power producing compartment, for example, by varying the pressure at which the working fluid boils while absorbing $\dot{Q}_H = \dot{m}c_p(T_H - T_{out}) = UA(T_{out} - T_s)$. When UA is sufficiently large, T_s is practically equal to T_{out}. In this case the optimal surface temperature is $T_{s,opt} = (T_H T_0)^{1/2}$, with the corresponding power output

$$\dot{W}_{\substack{\max \\ \text{Fig.2}}} = \dot{m}c_p T_0 \left[\left(\frac{T_H}{T_0} \right)^{1/2} - 1 \right]^2. \tag{2}$$

This power output is, as expected, smaller than in the reversible limit [equation (1)].

A more recent attempt to make the model of Fig. 1 more efficient is shown in Fig. 3 (ref. [8], p. 197). This figure has the same features as Fig. 2, except that the hot stream remains unmixed as it sweeps the heat transfer surface (UA, T_s). The heat input to the reversible compartment is $Q_H = \dot{m}c_p\varepsilon(T_H - T_s)$ where the heat exchanger effectiveness is $\varepsilon = 1 - \exp(-N_{tu})$, and $N_{tu} = UA/(\dot{m}c_p)$. It is not difficult to show that the optimal surface temperature is again $T_{s,opt} = (T_H T_0)^{1/2}$, and that the maximum power output is

$$\dot{W}_{\substack{\max \\ \text{Fig.3}}} = \dot{m}c_p T_0 \left[\left(\frac{T_H}{T_0} \right)^{1/2} - 1 \right]^2 [1 - \exp(-N_{tu})]. \tag{3}$$

This result is interesting for two reasons. First, it is smaller than in equation (2), in apparent contradiction of the fact that in going from Fig. 2 to Fig. 3 we have eliminated one source of irreversibility: the thermal mixing experienced by the hot stream in Fig. 2. The explanation is that equation (2) holds in the limit $N_{tu} \gg 1$. The second reason is that when the heat exchanger size (N_{tu}) becomes infinite equation (3) does not approach the reversible limit (1); instead, equation (3) approaches equation (2), which means that even when UA is infinite the model of Fig. 3 continues to generate entropy.

The three problems reviewed in Figs. 1–3 and equations (1)–(3) suggest that the question of how to maximize $\dot{W}$ subject to fixed heat exchanger size (UA) is considerably more interesting. To begin with, we should expect an answer ($\dot{W}_{max}$) that approaches the true ceiling value ($\dot{W}_{rev}$) as the heat exchanger size increases. Such an answer would also have practical value, because $\dot{W}_{rev}$ of equation (1) is considerably greater than the $UA \to \infty$ limit of the power output of the model of Fig. 3, equation (3). The objective of the following analysis is to identify in a fundamental way the optimal method of power delivery from a hot stream, when the heat exchanger inventory is finite.

2. NONISOTHERMAL HEAT TRANSFER SURFACE

In Figs. 1–3 and any other model, the hot stream becomes colder as it passes through the power plant. The heat transfer irreversibility of the power plant is due to two sources: (i) the temperature difference between the stream (T) and the heat exchanger surface (T_s), and (ii) the thermal mixing between the discharged stream (T_{out}) and the ambient (T_0). One way to decrease both sources is to allow the surface temperature to vary with (i.e. to follow) the hot stream temperature, and to lower the exhaust temperature closer to T_0.

These new features are evident in the power plant model defined by the solid line in Fig. 4. Temperature is plotted on the vertical. The length traveled by the hot stream (L) is proportional to the heat transfer area, $A = pL$, where p is the heat transfer area per unit of flow path length. The power producing compartment is a succession of many infinitesimal reversible compartments of the kind shown in the center of the figure. The infinitesimal power output is

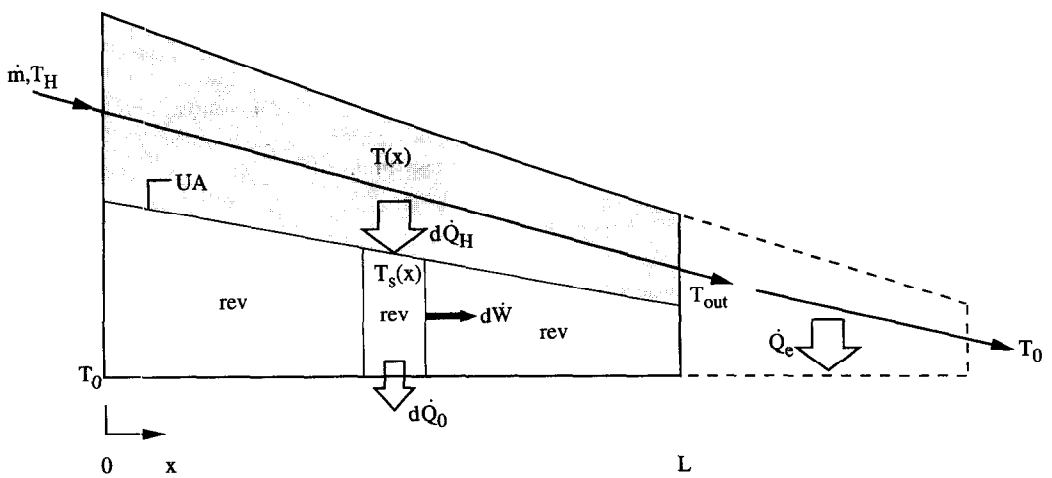

Fig. 4. Power plant model with unmixed hot stream in contact with a nonisothermal heat transfer surface.

$$d\dot{W} = \left[1 - \frac{T_0}{T_s(x)}\right] d\dot{Q}_H \tag{4}$$

where

$$d\dot{Q}_H = -\dot{m}c_p\, dT. \tag{5}$$

The heat transfer through the heat exchanger area is

$$d\dot{Q}_H = [T(x) - T_s(x)]Up\, dx. \tag{6}$$

Combining equations (5) and (6) and integrating from $x = 0$ to $x = L = A/p$ while treating U as a constant we arrive at a constraint that accounts for the finiteness of the heat exchanger area:

$$\int_{T_{out}}^{T_H} \frac{dT}{T - T_s} = \frac{UA}{\dot{m}c_p} = N_{tu}. \tag{7}$$

Similarly, by combining equations (4) and (5) we obtain the total power output

$$\dot{W} = \int_{T_{out}}^{T_H} \left(1 - \frac{T_0}{T_s}\right) \dot{m}c_p\, dT. \tag{8}$$

An alternate route to calculating the power output $\dot{W}$ is to apply the Gouy–Stodola theorem to the larger system (extended with dashed line) in Fig. 4:

$$\dot{W} = \dot{W}_{rev} - T_0 \dot{S}_{gen}. \tag{9}$$

The reversible-limit power output $\dot{W}_{rev}$ is the same as in Fig. 1 and equation (1), and corresponds to the reversible cooling of the stream from T_H all the way down to T_0. The entropy generation rate $\dot{S}_{gen}$ is the total amount associated with the larger system (Fig. 4), and is due to two sources: the temperature difference $T - T_s$, and the finite temperature difference required by the external cooling rate $\dot{Q}_e = \dot{m}c_p(T_{out} - T_0)$. These two contributions are represented by the two terms in the expression

$$\dot{S}_{gen} = \int_{T_{out}}^{T_H} \left(\frac{1}{T_s} - \frac{1}{T}\right) \dot{m}c_p\, dT + \left(\dot{m}c_p \ln \frac{T_0}{T_{out}} + \frac{\dot{Q}_e}{T_0}\right). \tag{10}$$

Note that the first term (the integral) comes from each infinitesimal power-producing element, $d\dot{S}_{gen} = d\dot{Q}_H/T_s - d\dot{Q}_H/T$ or $d\dot{S}_{gen} = d\dot{Q}_0/T_0 - d\dot{Q}_H/T$, because each element operates reversibly, $d\dot{Q}_H/T_s = d\dot{Q}_0/T_0$. The second term in equation (10) represents the irreversibility caused by discharging the T_{out} stream into the ambient.

In summary, equation (9) shows that to maximize $\dot{W}$ is equivalent to minimizing $\dot{S}_{gen}$, because $\dot{W}_{rev}$ is fixed. The entropy generation expression (10) is subject to the size constraint (7). There are two degrees of freedom in the minimization of $\dot{S}_{gen}$, first, the shape of the surface temperature function $T_s(x)$, and, second, the place of this function on the temperature scale (i.e., closer to T_H or T_0). The second degree of freedom is alternately represented by the value of the exhaust temperature T_{out}.

3. OPTIMAL SURFACE TEMPERATURE DISTRIBUTION

First, we assume that T_{out} has a specified value, and perform the optimization with respect to the shape of the function $T_s(x)$. When T_{out} is fixed, the only term that is free to vary in the $\dot{S}_{gen}$ expression (10) is the integral. To minimize this integral subject to the size constraint (7) is equivalent to finding the optimal function $T_{s,opt}$ for which the following aggregate integral reaches an extremum [9]:

$$\Phi = \int_{T_{out}}^{T_H} \left[\dot{m}c_p \left(\frac{1}{T_s} - \frac{1}{T}\right) + \lambda \frac{2}{T - T_s}\right] dT. \tag{11}$$

In this integral, the integrand (named F) is a linear combination of the integrands (10) and (7), and λ is a Lagrange multiplier. The optimal function $T_{s,opt}(T)$ is obtained by solving the Euler equation $\partial F/\partial T_s = 0$, which yields

$$T_{s,opt} = \mu T \tag{12}$$

where μ is a constant (related to λ) that can be determined by combining equation (12) with the size constraint (7):

$$\mu = 1 - \frac{1}{N_{tu}} \ln \frac{T_H}{T_{out}}. \tag{13}$$

Physically, we expect $\mu < 1$, which translates into $T_{out} < T_H$ for any N_{tu}.

The important conclusion made possible by equation (12) is that, after using equations (5) and (6), the optimal surface temperature distribution has an exponential-decay shape:

$$T_{s,opt}(x) = \mu T_H \exp\left(-\frac{x}{L} \ln \frac{T_H}{T_{out}}\right). \tag{14}$$

The corresponding stream temperature variation too as an exponential-decay shape,

$$T_{opt}(x) = T_H \exp\left(-\frac{x}{L} \ln \frac{T_H}{T_{out}}\right). \tag{15}$$

Equations (14) and (15) are illustrated for $N_{tu} = 3$ in Fig. 5. The maximum power output that corresponds to $T_{s,opt}$ is obtained by combining equations (12) and (8):

$$\dot{W}^{max}_{Fig.4} = \dot{m}c_p T_0 \left(\frac{T_H}{T_0} - \frac{T_{out}}{T_0} - \frac{1}{\mu} \ln \frac{T_H}{T_{out}}\right). \tag{16}$$

Together with the expression for μ [equation (13)], equation (16) delivers the dimensionless power output $\tilde{W}_m = \dot{W}_{max,Fig.4}/(\dot{m}c_p T_0)$ as a function of the overall temperature ratio (T_H/T_0), the finite size of the heat exchanger (N_{tu}), and the exhaust temperature that was assumed fixed (T_{out}/T_0).

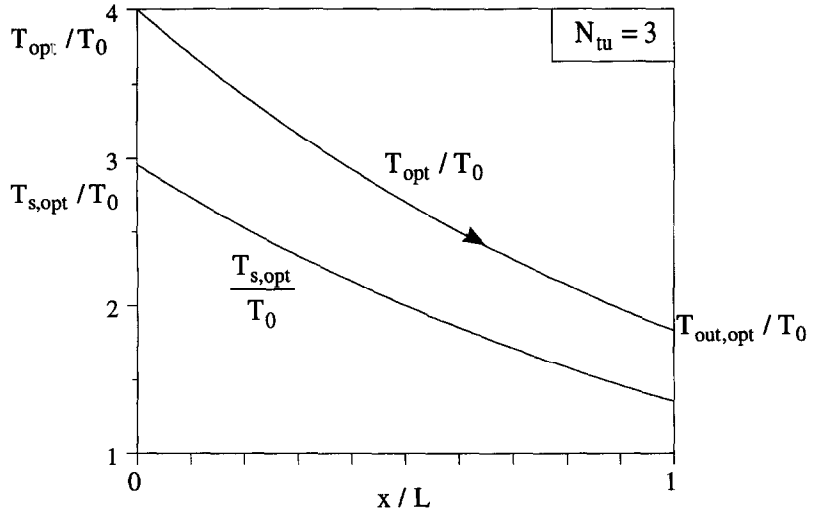

Fig. 5. The optimal distribution of temperature along the stream and the heat transfer surface in the model of Fig. 4.

4. OPTIMAL EXHAUST TEMPERATURE

The second step in the optimization procedure consists of maximizing the expression (16) with respect to T_{out}. The optimal exhaust temperature obtained by solving $\partial \dot{W}_{max,Fig.4}/\partial T_{out} = 0$ is given implicitly by

$$\frac{T_{out,opt}}{T_0}\left(1-\frac{1}{N_{tu}}\ln\frac{T_H}{T_{out,opt}}\right)^2 = 1. \tag{17}$$

Combining equations (17) and (13) we learn that $\mu = (T_0/T_{out,opt})^{1/2}$. Furthermore, since equation (12) also holds at $x = L$ [namely, $T_{s,opt}(L) = \mu T_{out,opt}$], we find that the trailing edge of the heat transfer surface must be warmer than the ambient,

$$T_{s,opt}(L) = \frac{1}{\mu}T_0. \tag{18}$$

The temperature distribution in the heat exchanger is now complete (Fig. 5). The surface temperature and the stream temperature decrease exponentially. The discharged stream carries exergy into the ambient: this exergy is destroyed through thermal mixing. Combining equations (16) and (17) we obtain the twice-maximized power output $\dot{W}_{mm,Fig.4}$. Its dimensionless counterpart,

$$\tilde{W}_{mm} = \frac{\dot{W}_{mm,Fig.4}}{\dot{m}c_p T_0} \tag{19}$$

is a function of only N_{tu} and T_H/T_0, and is reported in Fig. 6. As expected, the twice maximized power output increases monotonically with the source temperature (T_H/T_0). It can be verified that the second optimization step (with respect to T_{out}) led to an additional increase in the power output: this can be done numerically by comparing the twice maximized power of Fig. 6 with the once maximized power output of equation (16) in which we set, for example, $T_{s,opt} = T_0$ at $x = L$.

The maximum power output determined in this section ($\dot{W}_{mm}$) meets the criterion noted at the end of Section 1: in the infinite-size limit ($N_{tu} \to \infty$) μ approaches 1, $T_{out,opt}$ approaches T_0, and $\dot{W}_{mm}$ approaches $\dot{W}_{rev}$ of equation (1). This tendency is illustrated in Fig. 7, which shows the ratio $\dot{W}_{mm}/\dot{W}_{rev}$. Figure 7 shows that N_{tu} plays a more sensible role than T_H/T_0, and that $\dot{W}_{mm}$ approaches $\dot{W}_{rev}$ within less than 10% when N_{tu} exceeds 20.

Another instructive comparison is presented in Fig. 8, which shows the ratio between $\dot{W}_{mm}$ and the maximized power output of the scheme of Fig. 3, equation (3). Figure 8 shows the considerable gain in power output that is associated with the evolution from Fig. 3 to Fig. 4, i.e. the benefit derived from varying optimally the temperature (T_s) of the hot end of the reversible power cycle. This method of optimization is particularly effective when the heat exchanger is large, for example, when $N_{tu} \gtrsim 5$. It can be shown analytically that in the limit $N_{tu} \to \infty$ and $T_H/T_0 \to 1$ the ratio $\dot{W}_{mm}/\dot{W}_{max,Fig.3}$ is equal to 2. The overall temperature ratio T_H/T_0 has a relatively weak effect, especially when the N_{tu} value is not large.

5. COUNTERFLOW HEAT EXCHANGER AT THE HOT END

The optimization with respect to hot-end temperature distribution (Section 3) shows a way to implement the thermodynamic optimum in practice. Equation (12) means that at every position along the hot stream the temperature difference $T_{opt}(x) - T_{s,opt}(x)$ is proportional to the local absolute temperature

$$\left(\frac{T-T_s}{T_s}\right)_{opt} = \frac{1}{\mu} - 1. \tag{20}$$

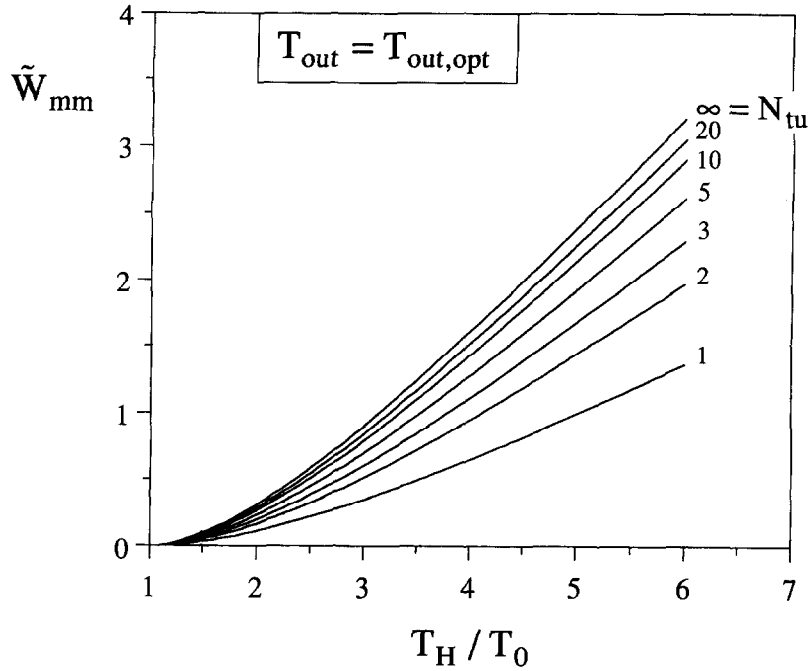

Fig. 6. The twice maximized power output corresponding to the optimal temperature distribution and the optimal outlet temperature [equations (14), (15) and (17)].

It happens that a proportionality of this type is also a feature in an unbalanced counterflow heat exchanger with constant capacity flow rates on both sides (e.g. ref. [7], p. 547). This means that one way to conceptualize a power plant design that approaches the arrangement analyzed in Fig. 4, is by running along the T_s surface a second stream $\dot{m}_s$ in counterflow with the source stream $\dot{m}$. The overall thermal conductance of the counterflow heat exchanger between $\dot{m}$ and $\dot{m}_s$ is UA.

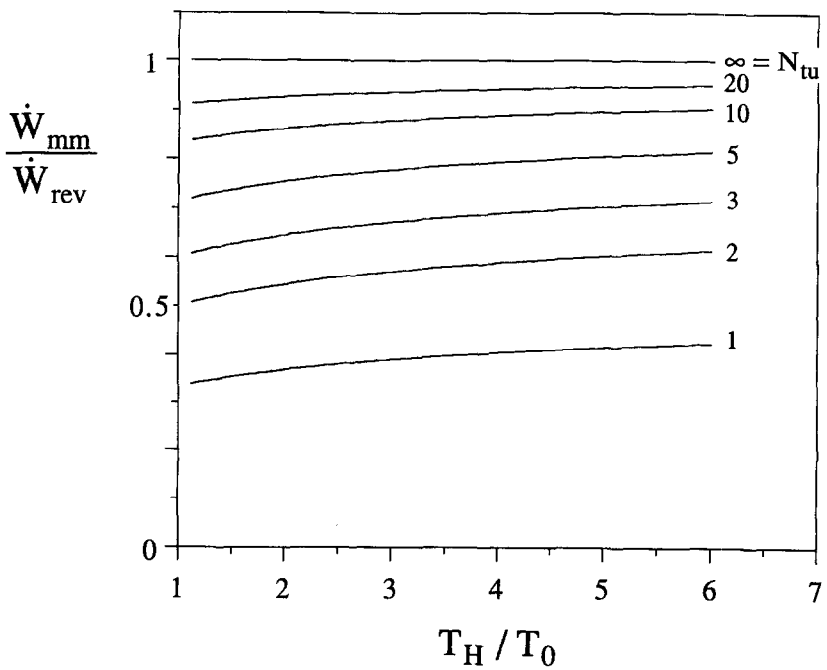

Fig. 7. Comparison between the twice maximized power output (Fig. 6) and the reversible power output of equation (1).

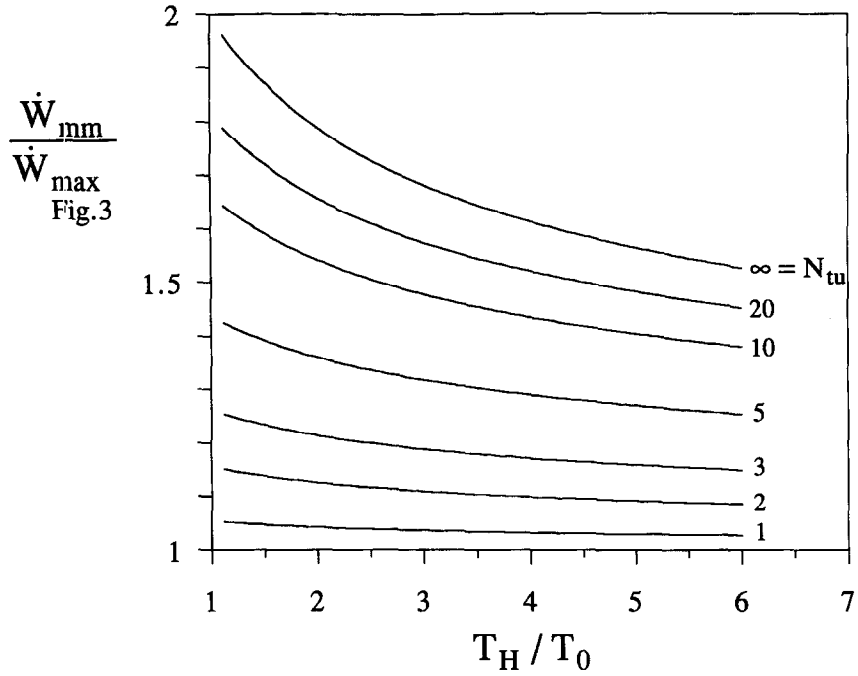

Fig. 8. Comparison between the twice maximized power (Fig. 6) and the maximized power of the model of Fig. 3.

The stream $\dot{m}_s$ is the working fluid of the reversibly operating device sketched between T_s and T_0 in Fig. 4. The capacity flow rate of this working fluid, $(\dot{m}c_p)_s$, can be found by invoking the first law in every infinitesimal slice dx of the counterflow heat exchanger,

$$\dot{m}c_p\,dT = (\dot{m}c_p)_s\,dT_s. \tag{21}$$

Combining equations (21) and (12) we obtain the ratio that describes the required unbalance of the counterflow heat exchanger,

$$\frac{(\dot{m}c_p)_s}{\dot{m}c_p} = \frac{1}{\mu} > 1. \tag{22}$$

According to Section 4, after the optimization of the second degree of freedom, μ is a known function of N_{tu} and T_H/T_0. In conclusion, the optimal capacity rate unbalance of the counterflow heat exchanger can be selected by using the $1/\mu$ function plotted in Fig. 9. The optimal unbalance is more pronounced when N_{tu} is small and T_H/T_0 is large.

6. COLD-END AND HOT-END HEAT EXCHANGERS

A step in the direction of making the model of Fig. 4 more realistic is the model shown in Fig. 10. This time we recognize that the rejected heat too requires a heat exchanger of finite size, $(UA)_L$. The role of heat sink is played by the single-phase cold stream of capacity rate $C_L = (\dot{m}c_p)_L$, which enters the power plant at the ambient temperature (T_L), and exits at $T_{c,out}$. The cold-stream temperature distribution along the $(UA)_L$ heat exchanger is $T_c(x)$. The cold-surface temperature of the reversible compartment is $T_{cr}(x)$.

For the hot-end heat exchanger we retain the model introduced in Section 2, except we use the notation $(UA)_H$ for the heat exchanger size, and $C_H = (\dot{m}c_p)_H$ for the capacity rate of the hot stream. These parameters are not necessarily equal to the corresponding parameters of the cold heat exchanger. The hot stream enters at T_H (fixed), exits at $T_{h,out}$, and its temperature variation is represented by $T_h(x)$. The temperature of the hot surface bathed by the hot stream is $T_{hr}(x)$. We use this notation to rewrite the optimal stream and surface temperature distributions derived in Section 2, namely equations (15) and (12):

$$T_h(x) = T_H \exp\left(-\frac{x}{L}\ln\frac{T_H}{T_{h,out}}\right) \tag{23}$$

$$T_{hr}(x) = \mu_H T_{h,opt}(x). \tag{24}$$

The $(UA)_H$ constraint written in place of equation (7) yields the relation between μ_H and the number of heat transfer units at the hot end $[N_H = (UA)_H/C_H]$, namely

$$\mu_H = 1 - \frac{1}{N_H}\ln\frac{T_H}{T_{h,out}} < 1. \tag{25}$$

The irreversibility minimization with respect to surface temperature (Section 3) can be repeated for the cold-end heat exchanger to arrive at conclusions equivalent to equations (15) and (12), respectively:

$$T_c(x) = T_{c,out}\exp\left(-\frac{x}{L}\ln\frac{T_{c,out}}{T_L}\right) \tag{26}$$

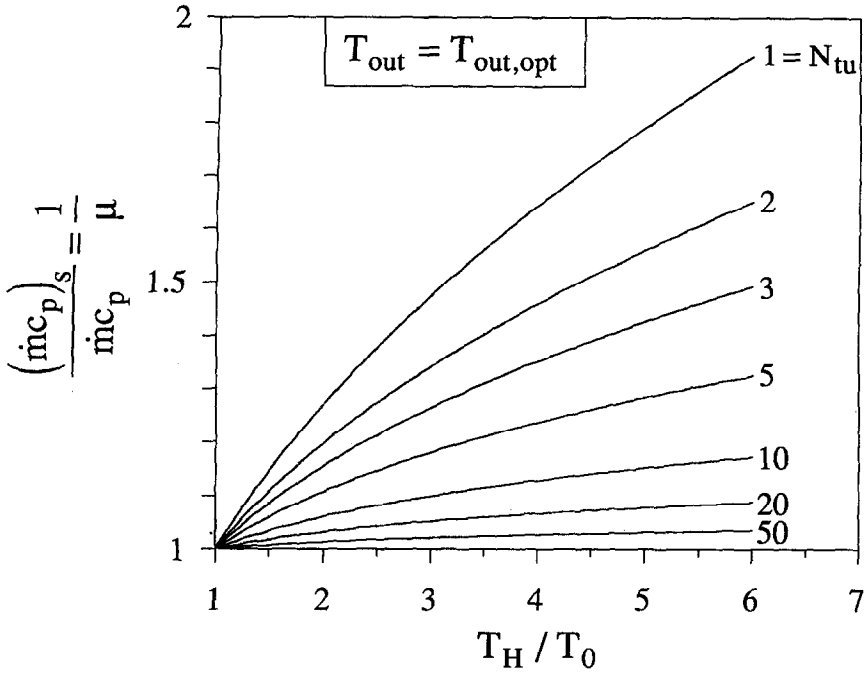

Fig. 9. The required imbalance of the counterflow heat exchanger used at the hot end of the model of Fig. 4.

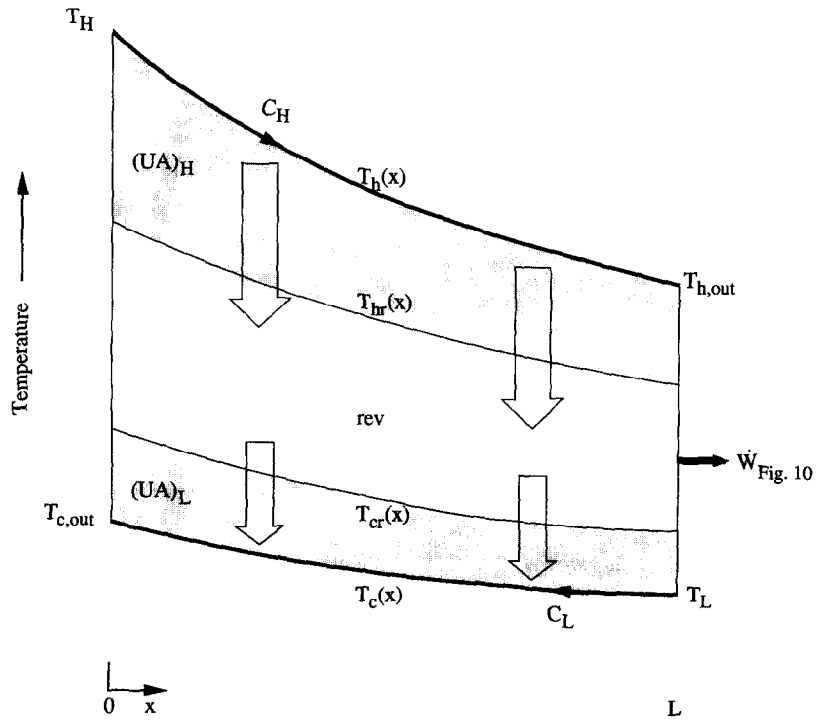

Fig. 10. Model of a power plant driven by two streams, one hot and the other cold.

$$T_{cr}(x) = \mu_L T_c(x). \tag{27}$$

The $(UA)_L$ constraint

$$\int_{T_L}^{T_{c,out}} \frac{dT_c}{T_{cr} - T_c} = \frac{(UA)_L}{C_L} N_L \tag{28}$$

established the relation between μ_L and the number of heat transfer units at the cold end (N_L),

$$\mu_L = 1 + \frac{1}{N_L} \ln \frac{T_{c,out}}{T_L} > 1. \tag{29}$$

This cold-end temperature distribution can be implemented by using a counterflow heat exchanger, as shown in Section 5.

The total power output from the model of Fig. 10 is obtained by combining the integral

$$\dot{W}_{Fig.10} = \int_{T_{h,out}}^{T_H} \left(1 - \frac{T_{cr}}{T_{hr}}\right) C_H \, dT_h \tag{30}$$

with equations (23), (24), (26) and (27). The resulting expression can be nondimensionalized as

$$\frac{\dot{W}}{C_H T_L} = \frac{T_H}{T_L} - \frac{T_{h,out}}{T_L} - \frac{\mu_L}{\mu_H} \left(\frac{T_{c,out}}{T_L} - 1\right) \frac{\ln(T_H/T_{h,out})}{\ln(T_{c,out}/T_L)}. \tag{31}$$

The outlet temperatures of the two streams and the power output are related through the first law of thermodynamics for the entire system of Fig. 10, which can be expressed as

$$\frac{\dot{W}}{C_H T_L} = \frac{T_H}{T_L} - \frac{T_{h,out}}{T_L} - \frac{C_L}{C_H} \left(\frac{T_{c,out}}{T_L} - 1\right). \tag{32}$$

In view of equations (25), (29), (31) and (32), the dimensionless power output $\hat{W} = \dot{W}/C_H T_L$ depends on five dimensionless numbers:

$$\frac{T_H}{T_L}, \quad N_H, \quad N_L, \quad \frac{C_L}{C_H}, \quad \frac{T_{h,out}}{T_L}. \tag{33}$$

The first four are fixed when the streams and the heat exchangers are specified. The fifth can be selected by maximizing $\hat{W}$ with respect to $T_{h,out}/T_L$. This operation was performed by nonlinear programming [10], and the results are illustrated in Fig. 11 for a finite C_L/C_H range. The maximized power output ($\hat{W}_{max}$) increases as the cold flow rate increases. At the same time, the two outlet temperatures decrease.

Another trade off in the maximization of power output is present when the total heat exchanger inventory is constrained $(UA)_H + (UA)_L = UA$ (constant) [7]. This constraint can be expressed in terms of N_H, N_L and C_L/C_H,

$$N_H + \frac{C_L}{C_H} N_L = N \tag{34}$$

where $N = UA/C_H$ is the overall number of heat transfer units. The maximized power output of Fig. 11, namely $\hat{W}_{max}(T_H/T_L, N_H, N_L, C_L/C_H)$, can be maximized once more by selecting the heat exchanger allocation ratio $\hat{x} = (UA)_H/UA$ subject to fixed N, T_H/T_L and C_L/C_H. Solving $\partial \hat{W}_{max}/\partial \hat{x} = 0$ we obtain

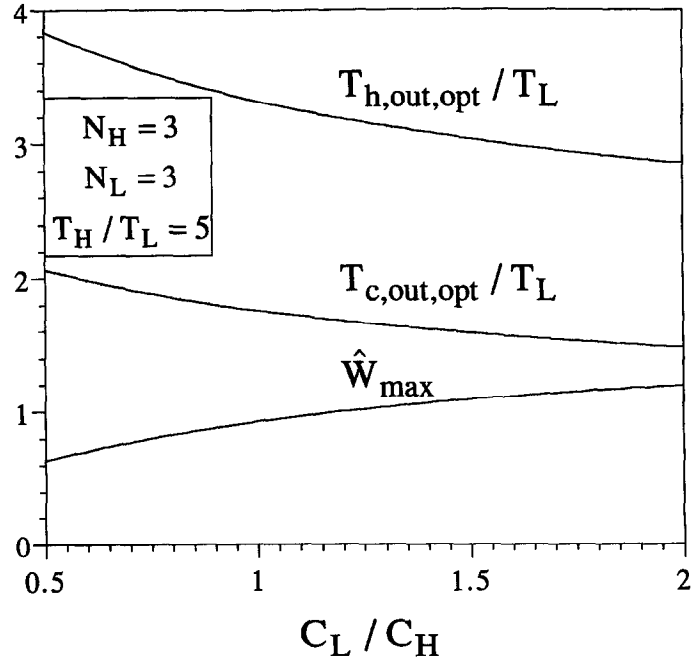

Fig. 11. The power output of the model of Fig. 10, maximized with respect to one of the outlet temperatures.

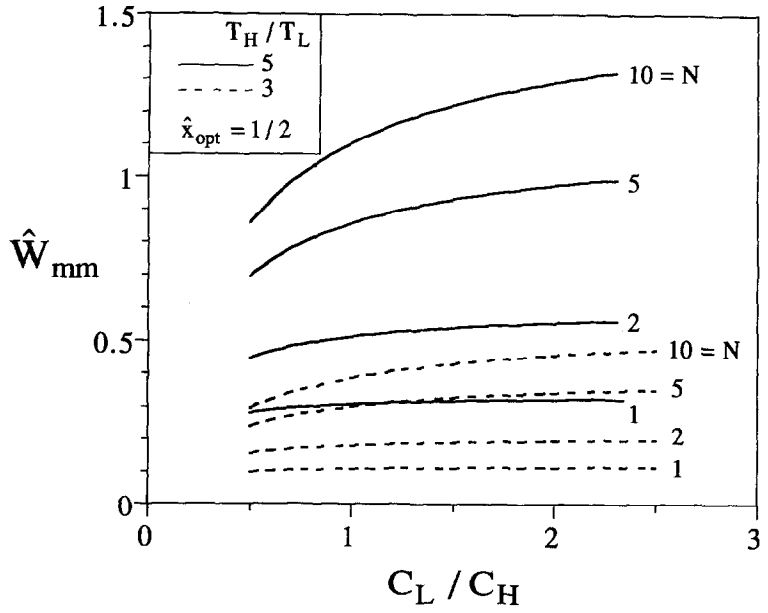

Fig. 12. The maximum power output of Fig. 11 maximized once more with respect to the UA allocation ratio $\hat{x}$.

$\hat{x}_{opt} = 1/2$, which means that the heat exchanger inventory should be divided exactly in half

$$(UA)_{H,opt} = (UA)_{L,opt} \tag{35}$$

regardless of the values of N, T_H/T_L and C_L/C_H. The maximized $\hat{W}_{max}$ values that correspond to $\hat{x}_{opt} = 1/2$ are shown as $\hat{W}_{mm}$ in Fig. 12. We see that $\hat{W}_{mm}$ increases monotonically with N, T_H/T_L and C_L/C_H. Note also that as N and T_H/T_L decrease, $\hat{W}_{mm}$ becomes practically insensitive to changes in C_L/C_H.

7. CONCLUSIONS

This paper outlined the solution to the fundamental problem of how to extract maximum power from a hot single-phase stream when the total heat transfer surface is fixed. The solution was obtained in two optimization steps. In the first, the shape of the stream temperature distribution (versus distance) was optimized. The result was an exponential stream temperature, and an exponential temperature distribution along the hot end of the reversible device that produces the power. The second step amounted to optimizing the positions of these temperature distributions on the absolute temperature scale. The double optimization problem was generalized to the case where the power plant (driven by the hot stream) relies on a cold single-phase stream for the heat rejection.

On the more practical side, this paper showed that the thermodynamic optimum can be achieved by using an appropriately imbalanced counterflow heat exchanger between the hot stream and the hot end of the cycle executed by the working fluid of the power producing device. The same heat exchanger type must be used at the cold end if heat is rejected to a single-phase cold stream. It must be said that the importance of counterflow heat exchangers, and of 'matching' the temperature of the working fluid to the temperature of the source stream is widely recognized in power engineering, for example, in Kalina-cycle power plants [11] a and combined-cycle power plants. The combined heat transfer and thermodynamic analysis constructed in this paper offers a compact and fundamental explanation for why these power engineering techniques are important.

Acknowledgements—This work was supported by the National Science Foundation, Air Force Office of Scientific Research and Conselho Nacional de Desenvolvimento Cientifico e Technologico, Brazil.

REFERENCES

1. Krane, R. J. ed., *Thermodynamics and the Design, Analysis, and Improvement of Energy Systems*. AES-Vol. 35, ASME, New York, 1995.
2. Krane, R. J. ed., *Thermodynamics and the Design, Analysis, and Improvement of Energy Systems*. AES-Vol. 33, ASME, New York, 1994.
3. Richter, H. J. ed., *Thermodynamics and the Design, Analysis, and Improvement of Energy Systems*. HTD-Vol. 266, ASME, New York, 1993.
4. Moran, M. J. and Sciubba, E., Exergetic analysis: principles and practice. *J. Eng. Gas Turbines Power*, 1994, **116**, 285–290.
5. Stecco, S. S. and Moran, M. J., *Energy for the Transition Age*. Nova Science, New York, 1992.
6. Bejan, A., *Entropy Generation through Heat and Fluid Flow*. Wiley, New York, 1982.
7. Bejan, A., *Advanced Engineering Thermodynamics*. Wiley, New York, 1988.
8. Bejan, A., *Entropy Generation Minimization*. CRC Press, Boca Raton, 1996.

9. Hildebrand, F. B., *Advanced Calculus for Applications*. Prentice-Hall, Englewood Cliffs, NJ, 1962.
10. Bazaraa, M. and Shetty, C. M., *Nonlinear Programming*. Wiley, New York, 1979.
11. El-Sayed, Y. M. and Tribus, M., A theoretical comparison of the Rankine and Kalina cycles. In *Analysis of Energy Systems—Design and Operation*, ed. R. A. Gaggioli. AES-Vol. 1, ASME, New York, 1985.